Rapid Communications

Onset of a skyrmion phase by chemical substitution in MnGe-based chiral magnets

E. Altynbaev,[1,2] N. Martin,[3] A. Heinemann,[4] L. Fomicheva,[2] A. Tsvyashchenko,[2] I. Mirebeau,[3] and S. Grigoriev[1,2,5]

[1]*Petersburg Nuclear Physics Institute National Research Center "Kurchatov Institute," Gatchina, 188300 St. Petersburg, Russia*

[2]*Vereshchagin Institute for High Pressure Physics, Russian Academy of Sciences, 142190 Troitsk, Moscow, Russia*

[3]*Université Paris-Saclay, CNRS, CEA, Laboratoire Léon Brillouin, 91191 Gif-sur-Yvette, France*

[4]*Helmholtz Zentrum Geesthacht, 21502 Geesthacht, Germany*

[5]*Faculty of Physics, Saint-Petersburg State University, 198504 St. Petersburg, Russia*

(Received 11 September 2019; revised manuscript received 5 February 2020; accepted 28 February 2020; published 13 March 2020)

We study the evolution of the magnetic phase diagram of $Mn_{1-x}Fe_xGe$ alloys with concentration x ($0 \leqslant x \leqslant 0.3$) by small-angle neutron scattering. We unambiguously observe the absence of a skyrmion (Sk) lattice (or A phase) in bulk MnGe and its onset under a small Mn/Fe substitution. The A phase is there endowed with extremely small Sks, potentially resulting in a high density, and is stabilized within a very large temperature region and a field range which scales with the Fe concentration. Our findings highlight the possibility to fine tune the properties of skyrmion lattices by means of chemical doping.

DOI: 10.1103/PhysRevB.101.100404

Introduction. The incommensurate magnetic orderings of alloys with a B20 structure, such as MnSi or FeGe, have received increasing attention in the last decade due to their peculiar magnetotransport properties. Their helical spin structure results from a competition between the ferromagnetic (FM) exchange and antisymmetric Dzyaloshinskii-Moriya interaction (DMI), allowed by the lack of inversion symmetry in the crystal structure [1–4]. The presence of helical Bragg peaks in the direction perpendicular to the applied field $\mathbf{H}$, initially discovered in bulk MnSi single crystals by small-angle neutron scattering (SANS) [5,6], was later on ascribed to a stacking of two-dimensional lattice of magnetic defects called "skyrmions" (Sks) [7]. The Sk lattice, a hexagonal pattern with wave vector $\mathbf{k}_A \perp \mathbf{H}$, was further observed in real space by Lorentz transmission electron microscopy (TEM) [8]. Recent theories show that it results from uniaxial anisotropy, due to DMI in the bulk or interfaces in layers, both reducing the effective symmetry [9]. In B20 metallic magnets, such as $Mn_{1-x}Fe_xSi$, $Fe_{1-x}Co_xSi$, and $Fe_{1-x}Co_xGe$, a stable Sk lattice is only observed in the bulk state in a limited (H, T) region, situated just below the ordering temperature T_C, the so-called "A phase." This suggests that chiral fluctuations, numerous around T_C [10–12], are needed for its stabilization together with the DMI term. Although anisotropy may induce stable Sks at low temperature in bulk systems [13,14], they have only been observed in multiferroic Cu_2OSeO_3 [15,16] with a rather different crystal structure and transport properties.

In the B20 family, the MnGe helical magnet synthesized in a metastable form under high pressure and temperature [17] stands as an exception. MnGe orders at high temperature ($T_C \approx 170$ K) with a much shorter helical wavelength ($\lambda_s = 2\pi/k_s \approx 3$–$6$ nm) [18,19] than MnSi or FeGe. This strongly suggests that sizable next-nearest antiferromagnetic (AFM) interactions are responsible for the helical structure [20,21]. MnGe also exhibits a magnetic order-disorder transition spanning a large temperature range [22], and involving low-energy spin fluctuations [23,24]. In MnGe, a possible Sk lattice was inferred from SANS [25] and TEM [26] studies. In the initial SANS experiments of Kanazawa *et al.* [25], the intensity peak attributed to the A phase was observed after the application of a large field, that could orient not only the magnetic but also the crystal domains along the field direction. Therefore an alternative scenario involving helices blocked in the hard directions could explain such intensity. On the other hand, observations of the Sk lattice by TEM [26] may be impacted by a multidomain structure of helices oriented along the edges of the cubic unit cell or by surface anisotropy. Therefore the Sk lattice in MnGe remains elusive and exotic monopole defects have been further proposed [27].

Remarkably, *ab initio* calculations show that the DMI term is close to zero in MnGe, and increases under Mn/Fe substitution [28,29]. In $Mn_{1-x}Fe_xGe$ compounds, the ground-state helical structure remains essentially similar up to $x = 0.35$ [30], but the borders of the A phase have not yet been directly observed. Therefore, the Mn-rich $Mn_{1-x}Fe_xGe$ compounds are of great interest to study the influence of the DMI term on the stability of the Sk lattice.

In this Rapid Communication, we present a comprehensive SANS study of the magnetic structure of $Mn_{1-x}Fe_xGe$ compounds with $0 \leqslant x \leqslant 0.3$ under an applied magnetic field. We have used the same protocol for all samples, a well-defined procedure allowing one to determine the boundaries of the A phase without ambiguity. We find that pure MnGe does not show any traces of a Sk lattice within the explored temperature ($T \leqslant 200$ K) and field ($0 \leqslant H \leqslant 9$ T) ranges. In turn, the substitution of Mn ions by Fe ions results in the appearance of an A phase, with Sks having the shortest period among the materials stabilizing such structures. This phase extends over a wide temperature range, almost independent of x, whereas its field range *increases* with x. The latter scales with the calculated DMI term. Our finding agrees with the theoretical calculation of an almost zero DMI term in MnGe,

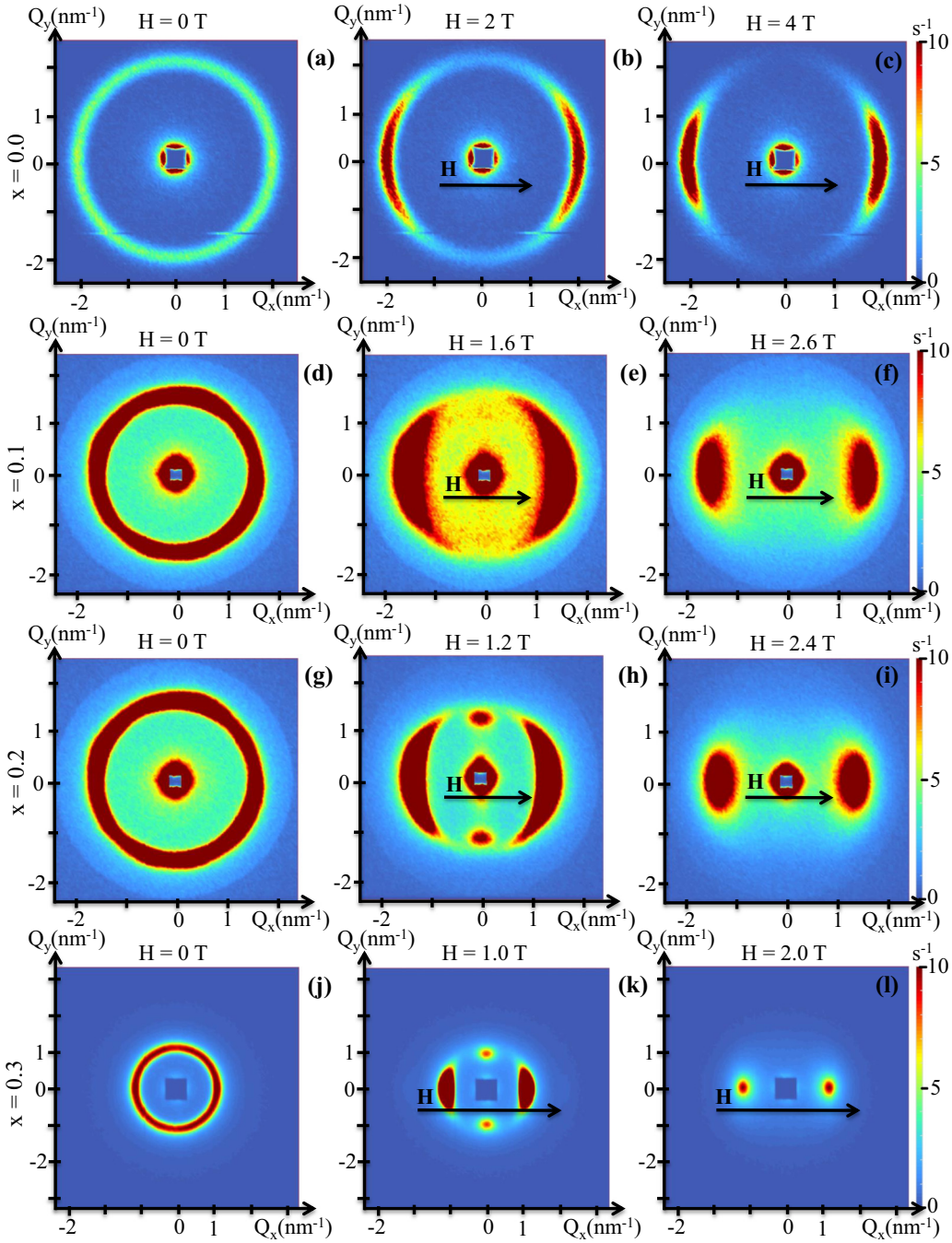

FIG. 1. Small-angle scattering intensity maps, taken at different fields at $T = 90$ K on MnGe (a)–(c) and $T = 100$ K on $Mn_{1-x}Fe_xGe$ compounds with $x = 0.1$ (d)–(f), 0.2 (g)–(i), and 0.3 (j)–(l).

and supports the *A* phase as an inherent feature of DMI helimagnets.

Experimental results. Polycrystalline $Mn_{1-x}Fe_xGe$ samples were previously used in Ref. [21]. Details on their synthesis are given in the Supplemental Material [31]. SANS experiments were carried out on the SANS-1 instrument at the Heinz Maier-Leibnitz Institute (MLZ, Garching, Germany [32]) and on the PA20 instrument at the Laboratoire Léon Brillouin (LLB, Saclay, France [33]), covering momentum transfers in the range $0.2 \leqslant Q \leqslant 2.7$ nm^{-1}. The scattered intensity was systematically measured *after zero-field cooling* from $T = 300$ K (in the paramagnetic state) down to the chosen temperature, and upon a gradual increase of the magnetic field up to 9 T.

Figure 1 shows examples of SANS maps taken at different fields at $T = 90$ K on MnGe and $T = 100$ K on $Mn_{1-x}Fe_xGe$ compounds. In pure MnGe [Figs. 1(a)–1(c)], the isotropic ring observed in zero field transforms into a moonlike pattern oriented along the field, as expected from the evolution of the helical structure towards the conical one. However, we do not observe peaks in the direction perpendicular to the field, regardless of the field and temperature up to 9 T and 200 K.

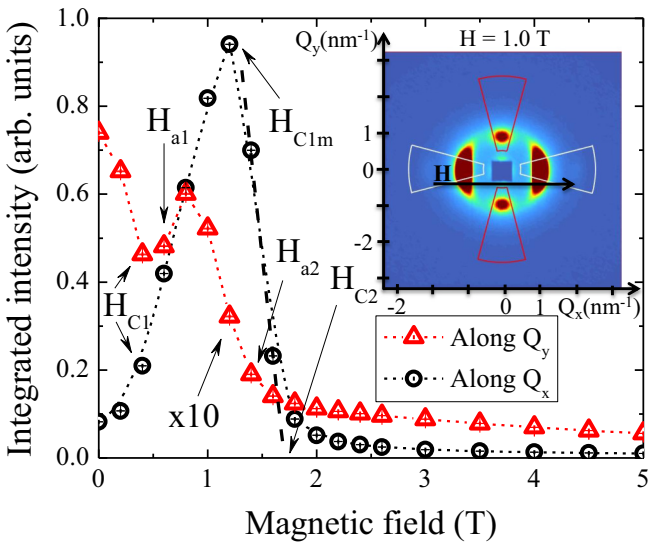

FIG. 2. Neutron scattering intensity deduced from the SANS maps of $Mn_{0.7}Fe_{0.3}Ge$, integrated in directions along (black circles) and perpendicular (red triangles) to the external field H at $T = 100$ K. A map measured at 100 K and 0.8 T is shown in the inset with the white (red) integration sector for the direction along (perpendicular to) the magnetic field.

The latter are the usual hallmark of the A phase, within which the longitudinal magnetization is modulated in the form of a Sk lattice. Strikingly, they appear in the substituted samples starting from the lowest concentration $x = 0.1$, as a weak signal superimposed on the ring structure [Figs. 1(d)–1(f)]. The spots from the A phase become better defined for the samples with $x = 0.2$ and 0.3 [Figs. 1(g)–1(i) and 1(j)–1(l), respectively). They directly demonstrate the transition of part of the samples into the A phase and the emergence of Sk lattices.

In order to determine the (H, T) phase diagrams of the studied samples, the neutron scattering intensities were integrated in the horizontal or vertical directions over the azimuthal angle of 30°, i.e., longitudinal or transverse to the applied field, respectively. From the field dependence of the intensity at a given temperature, up to five characteristic fields can be deduced, as shown in Fig. 2 for $x = 0.3$ at $T = 100$ K. The critical field H_{C1}, which we consider as the field value where the longitudinal and transverse intensities differ by more than 20%, indicates the departure from the multidomain helical state. The field H_{C1m}, where the longitudinal intensity reaches its maximum, marks the end of this reorientation process and the transition of each sample grain into a single domain conical state. The critical field H_{C2}, determined by extrapolating to zero the linear decay of the longitudinal intensity with the field increase above H_{C1m}, marks the transition from the conical to the field-induced ferromagnetic state. The fields H_{a1} and H_{a2} are determined as the borders of the field range where the intensity in the direction, transverse to the external field, increases, indicating the Sk peaks to emerge from the ringlike signal. These fields correspond to the lower and upper limit of the A phase, respectively. Details on the accurate determination of the values of H_{a1} and H_{a2} are given in the Supplemental Material [31]. The resulting (H, T) phase diagrams are shown in Fig. 3(a) for MnGe and Figs. 3(b)–3(d) for the substituted compounds.

In Fig. 3(e), we plot the quantity H_{a2}-H_{a1} which marks the field extension of the A phase for each concentration versus the DMI constant D deduced from *ab initio* calculations. The error bars on H_{a2}-H_{a1} take into account its temperature dependence, whereas the DMI constant is averaged over several theoretical works [28,34,35]. Both quantities have negligible values for pure MnGe, and are linearly increasing with concentration x within error bars.

The positions of the Bragg reflections yield the periodicity of the helical structure and of the Sk lattice. They can be determined for each sample as a function of field and temperature. The wave vectors of the helical structure (k_s) and Sk lattice (k_A) are almost independent of the applied field. They slowly increase with decreasing temperature, in the same way for each sample [Fig. 3(f)]. Strikingly, their ratio (k_A/k_s) remains almost constant, independent of the temperature and sample considered, close to the value $k_A/k_s \approx 0.866 \approx \sqrt{3}/2$.

Discussion. In pure MnGe, the critical fields measured at low temperature $H_{C1} \approx 3$ T and $H_{C1m} \approx 5$ T are the highest measured in B20 compounds so far. Upon heating, they decrease to zero at $T \approx 190$ K [Fig. 3(a)]. As a main result, we find no traces of the Sk lattice when performing a careful search in the whole (H, T) range up to 9 T and 200 K. The critical field H_{C2} decreases linearly upon heating down to 3 T at $T = 150 \pm 2$ K, then saturates and remains constant up to 190 K. As long as the traces of the helical structure persist up to 190 K, the temperature range 150–190 K likely consists of a mixed state where helical fluctuations and ferromagnetic nanoregions coexist in the sample [22].

In the substituted compounds $Mn_{1-x}Fe_xGe$ with $x = 0.1$, 0.2, and 0.3 [Figs. 3(b)–3(d)], the temperature variation of the critical fields H_{C1}, H_{C1m}, and H_{C2} is similar to that of MnGe. H_{C1} and H_{C1m} are almost independent of x and decrease to zero at $T \approx 160$ K. The main difference with MnGe is the occurrence of an A phase in a wide (T, H) range. It is observed for 20 K $< T <$ 120 K ($x = 0.1$) and 40 K $< T <$ 140 K (for $x = 0.2, 0.3$). The A phase extends widely in the oriented helical phase, between H_{C1} and H_{C1m} ($x = 0.1, 0.2$), or slightly above H_{C1m} ($x = 0.3$). The large extension of the A phase with temperature likely results from the intrinsic instability of $Mn_{1-x}Fe_xGe$ [21–23,36,37], favoring helical fluctuations well below the ordering temperature. The A phase persists up to T_N, i.e., when long-range helical order is stable. It vanishes at higher temperatures, in a region where finite-size ferromagnetic correlations are observed, while critical fields can still be defined. Strikingly, in these Mn-rich compounds where the temperature extension of the A phase does not depend much on x, its field extension H_{a2}-H_{a1} increases with x, in a linear way (within error bars), as does the calculated DMI constant [28,34,35]. The proportional increase of these two quantities [Fig. 3(e)] supports the DMI as the fundamental interaction needed to stabilize the A phase in bulk B20 magnets.

The difference between the wave vectors of the helical structure and Sk lattice $k_A/k_s \approx 0.866$ is surprising. It means that the period of the Sk is bigger than the period of the helical structure by almost 15% regardless of the concentration

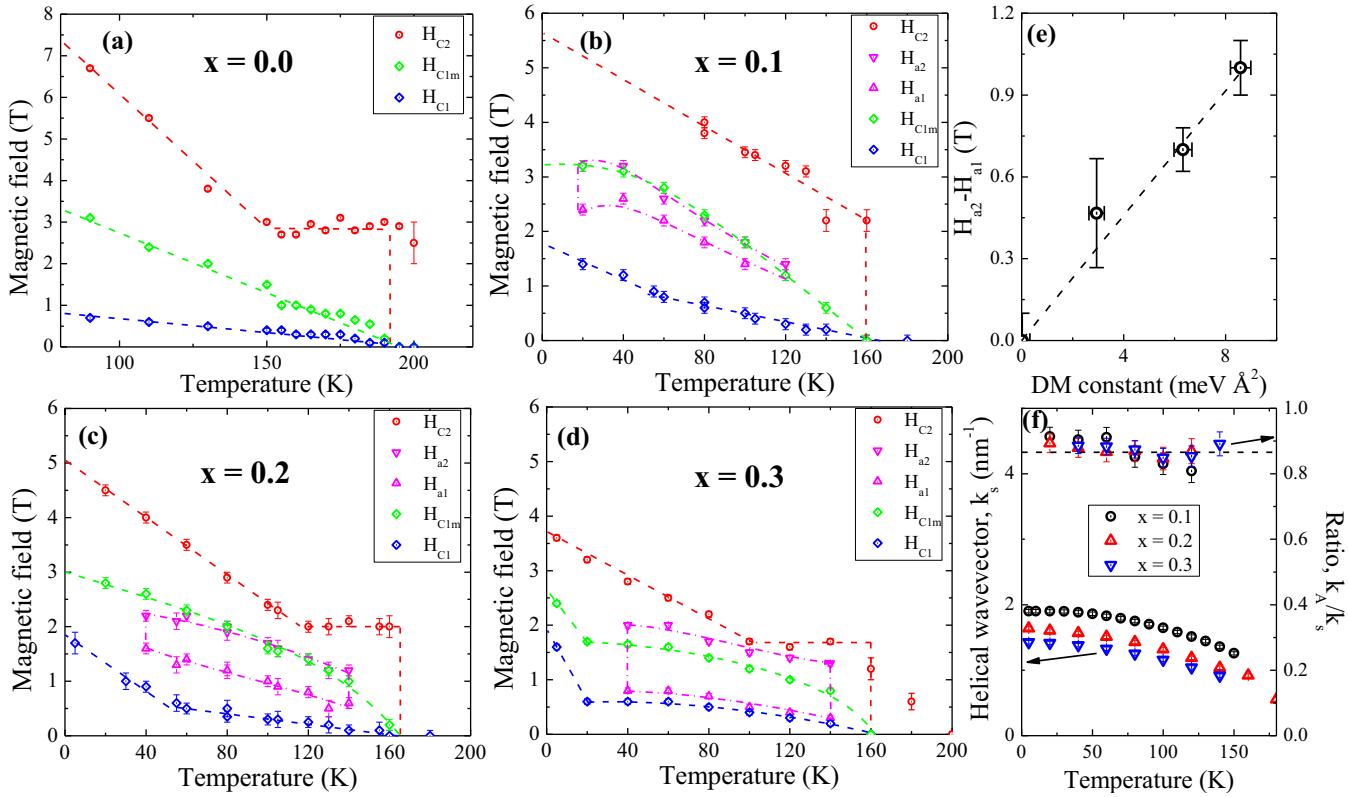

FIG. 3. (H, T) phase diagrams of $Mn_{1-x}Fe_xGe$, with $x = 0.0$ (a), 0.1 (b), 0.2 (c), and 0.3 (d). (e) Field extension of the A phase (averaged over temperature for each sample) vs the calculated DMI constant [28,29,34,35]. The dashed line is the linear fit of the width of the A-phase vs DMI-constant plot with intercept equal to zero. (f) Temperature dependence of the helical wave vector k_s (left) and ratio of the wave vector k_A of the A phase over k_s, k_A/k_s (right), for all samples.

and temperature. We should also note that simple geometric arguments in the case of a hexagonal Sk lattice imply an opposite ratio, namely, $k_s/k_A = \sqrt{3}/2$ [38]. However, it is found experimentally that $k_s = k_A$ within 1%–2%, either in bulk [5,6,39] or in two-dimensional [8,40] helimagnets, with the exception of the frustrated disordered Co-Zn-Mn alloys [41]. Nevertheless, the observed ratio between k_A and k_s could suggest that the Sks found within the A phase of $Mn_{1-x}Fe_xGe$ ($x \geqslant 0.1$) are not packed in a regular hexagonal fashion. We thus speculate that the observed difference might be related to the competition between FM and AFM exchange interactions or to chemical disorder (or both). This point deserves further theoretical and experimental studies.

The absence of a regular Sk lattice in bulk MnGe suggests one to reinterpret the first investigations of its (H, T) phase diagram [25,26]. The traces of the Sk lattice observed earlier could also be explained as an experimental artifact. On the other hand, the absence of the Sk lattice in bulk MnGe is fairly natural from a theoretical viewpoint, taking into account the vanishingly small value of its DM constant. The question that remains open concerns the origin of the large topological Hall effect (THE). Besides Sks, other topological objects have been proposed in MnGe, such as monopole [27] or soliton defects [24], owing to its intrinsic instability [22,23,36]. They may provide another source for the THE.

Conclusion. We have observed the absence of a regular Sk lattice or A phase in MnGe and its onset under a small substitution of Mn for Fe. The A phase is observed over a wide temperature range, perhaps owing to the inherent fluctuations and metastable character of $Mn_{1-x}Fe_xGe$. Its field range increases linearly with the Fe concentration and calculated DMI constant. These results emphasize that DMI and helical fluctuations are the main ingredients for the stabilization of a Sk lattice in B20 magnets, and indicate a way to fine tune the properties of a dense Sk lattice using controlled chemical substitution.

Acknowledgments. E.A., A.T., and S.G. are grateful to the Russian Scientific Foundation (Grant No. 17-12-01050).

[1] Y. Ishikawa, K. Tajima, D. Bloch, and M. Roth, Solid State Commun. **19**, 525 (1976).

[2] B. Lebech, J. Bernhard, and T. Freltoft, J. Phys.: Condens. Matter **1**, 6105 (1989).

[3] O. Nakanishi, A. Yanase, A. Hasegawa, and M. Kataoka, Solid State Commun. **35**, 995 (1980).

[4] P. Bak and M. H. Jensen, J. Phys. C: Solid State Phys. **13**, L881 (1980).

[5] B. Lebech, P. Harris, J. S. Pedersen, K. Mortensen, C. Gregory, N. Bernhoeft, M. Jermy, and S. Brown, J. Magn. Magn. Mater. **140-144**, 119 (1995).

[6] S. V. Grigoriev, S. V. Maleyev, A. I. Okorokov, Y. O. Chetverikov, and H. Eckerlebe, Phys. Rev. B **73**, 224440 (2006).

[7] S. Mühlbauer, B. Binz, F. Jonietz, C. Pfleiderer, A. Rosch, A. Neubauer, R. Georgii, and P. Böni, Science **323**, 915 (2009).

[8] X. Z. Yu, Y. Onose, N. Kanazawa, J. H. Park, J. H. Han, Y. Matsui, N. Nagaosa, and Y. Tokura, Nature (London) **465**, 901 (2010).

[9] F. N. Rybakov, A. B. Borisov, S. Blügel, and N. S. Kiselev, Phys. Rev. Lett. **115**, 117201 (2015).

[10] S. V. Grigoriev, S. V. Maleyev, A. I. Okorokov, Y. O. Chetverikov, R. Georgii, P. Böni, D. Lamago, H. Eckerlebe, and K. Pranzas, Phys. Rev. B **72**, 134420 (2005).

[11] S. V. Grigoriev, E. V. Moskvin, V. A. Dyadkin, D. Lamago, T. Wolf, H. Eckerlebe, and S. V. Maleyev, Phys. Rev. B **83**, 224411 (2011).

[12] M. Janoschek, M. Garst, A. Bauer, P. Krautscheid, R. Georgii, P. Böni, and C. Pfleiderer, Phys. Rev. B **87**, 134407 (2013).

[13] T. Okubo, S. Chung, and H. Kawamura, Phys. Rev. Lett. **108**, 017206 (2012).

[14] A. O. Leonov and M. Mostovoy, Nat. Commun. **6**, 8275 (2015).

[15] A. Chacon, L. Heinen, M. Halder, A. Bauer, W. Simeth, S. Mühlbauer, H. Berger, M. Garst, A. Rosch, and C. Pfleiderer, Nat. Phys. **14**, 936 (2018).

[16] L. J. Bannenberg, H. Wilhelm, R. Cubitt, A. Labh, M. P. Schmidt, E. Lelièvre-Berna, C. Pappas, M. Mostovoy, and A. O. Leonov, npj Quantum Mater. **4**, 11 (2019).

[17] A. V. Tsvyashchenko, V. A. Sidorov, L. N. Fomicheva, V. N. Krasnorussky, R. A. Sadykov, J. D. Thompson, K. Gofryk, F. Ronning, and V. Yu. Ivanov, in *Magnetism and Magnetic Materials V*, edited by N. Perov and V. Rodionova, Solid State Phenomena Vol. 190 (Trans Tech, Baech, Switzerland, 2012), pp. 225–228.

[18] O. L. Makarova, A. V. Tsvyashchenko, G. Andre, F. Porcher, L. N. Fomicheva, N. Rey, and I. Mirebeau, Phys. Rev. B **85**, 205205 (2012).

[19] N. Kanazawa, Y. Onose, T. Arima, D. Okuyama, K. Ohoyama, S. Wakimoto, K. Kakurai, S. Ishiwata, and Y. Tokura, Phys. Rev. Lett. **106**, 156603 (2011).

[20] V. A. Chizhikov and V. E. Dmitrienko, Phys. Rev. B **88**, 214402 (2013).

[21] E. Altynbaev, S.-A. Siegfried, E. Moskvin, D. Menzel, C. Dewhurst, A. Heinemann, A. Feoktystov, L. Fomicheva, A. Tsvyashchenko, and S. Grigoriev, Phys. Rev. B **94**, 174403 (2016).

[22] E. Altynbaev, S.-A. Siegfried, V. Dyadkin, E. Moskvin, D. Menzel, A. Heinemann, C. Dewhurst, L. Fomicheva, A. Tsvyashchenko, and S. Grigoriev, Phys. Rev. B **90**, 174420 (2014).

[23] N. Martin, M. Deutsch, F. Bert, D. Andreica, A. Amato, P. Bonfà, R. De Renzi, U. K. Rößler, P. Bonville, L. N. Fomicheva *et al.*, Phys. Rev. B **93**, 174405 (2016).

[24] N. Martin, I. Mirebeau, C. Franz, G. Chaboussant, L. N. Fomicheva, and A. V. Tsvyashchenko, Phys. Rev. B **99**, 100402(R) (2019).

[25] N. Kanazawa, J.-H. Kim, D. S. Inosov, J. S. White, N. Egetenmeyer, J. L. Gavilano, S. Ishiwata, Y. Onose, T. Arima, B. Keimer *et al.*, Phys. Rev. B **86**, 134425 (2012).

[26] T. Tanigaki, K. Shibata, N. Kanazawa, X. Yu, Y. Onose, H. S. Park, D. Shindo, and Y. Tokura, Nano Lett. **15**, 5438 (2015).

[27] N. Kanazawa, Y. Nii, X. X. Zhang, A. S. Mishchenko, G. De Filippis, F. Kagawa, Y. Iwasa, N. Nagaosa, and Y. Tokura, Nat. Commun. **7**, 11622 (2016).

[28] J. Gayles, F. Freimuth, T. Schena, G. Lani, P. Mavropoulos, R. A. Duine, S. Blügel, J. Sinova, and Y. Mokrousov, Phys. Rev. Lett. **115**, 036602 (2015).

[29] T. Koretsune, T. Kikuchi, and R. Arita, J. Phys. Soc. Jpn. **87**, 041011 (2018).

[30] S. V. Grigoriev, N. M. Potapova, S.-A. Siegfried, V. A. Dyadkin, E. V. Moskvin, V. Dmitriev, D. Menzel, C. D. Dewhurst, D. Chernyshov, R. A. Sadykov *et al.*, Phys. Rev. Lett. **110**, 207201 (2013).

[31] See Supplemental Material at http://link.aps.org/supplemental/10.1103/PhysRevB.101.100404 for details about the samples and the analysis strategies used in this study, which includes Refs. [42,43].

[32] A. Heinemann and S. Mühlbauer, J. Large-Scale Res. Facil. **1**, A10 (2015).

[33] G. Chaboussant, S. Désert, P. Lavie, and A. Brûlet, J. Phys.: Conf. Ser. **340**, 012002 (2012).

[34] T. Kikuchi, T. Koretsune, R. Arita, and G. Tatara, Phys. Rev. Lett. **116**, 247201 (2016).

[35] S. Mankovsky, S. Wimmer, S. Polesya, and H. Ebert, Phys. Rev. B **97**, 024403 (2018).

[36] M. Deutsch, P. Bonville, A. V. Tsvyashchenko, L. N. Fomicheva, F. Porcher, F. Damay, S. Petit, and I. Mirebeau, Phys. Rev. B **90**, 144401 (2014).

[37] E. V. Altynbaev, A. S. Sukhanov, S.-A. Siegfried, V. A. Dyadkin, E. V. Moskvin, D. Menzel, A. Heinemann, A. Schreyer, L. N. Fomicheva, A. V. Tsvyashenko *et al.*, J. Surf. Invest.: X-Ray, Synchrotron Neutron Tech. **10**, 777 (2016).

[38] S. V. Grigoriev, N. M. Potapova, E. V. Moskvin, V. A. Dyadkin, C. Dewhurst, and S. V. Maleyev, JETP Lett. **100**, 216 (2014).

[39] K. Ishimoto, H. Yamauchi, Y. Yamaguchi, J. Suzuki, M. Arai, M. Furusaka, and Y. Endoh, J. Magn. Magn. Mater. **90-91**, 163 (1990).

[40] A. Tonomura, X. Yu, K. Yanagisawa, T. Matsuda, Y. Onose, N. Kanazawa, H. S. Park, and Y. Tokura, Nano Lett. **12**, 1673 (2012).

[41] K. Karube, J. S. White, N. Reynolds, J. L. Gavilano, H. Oike, A. Kikkawa, F. Kagawa, Y. Tokunaga, H. M. Rønnow, Y. Tokura *et al.*, Nat. Mater. **15**, 1237 (2016).

[42] V. Dyadkin, S. Grigoriev, S. V. Ovsyannikov, E. Bykova, L. Dubrovinsky, A. Tsvyashchenko, L. Fomicheva, and D. Chernyshov, Acta Crystallogr., Sect. B **70**, 676 (2014).

[43] G. A. Valkovskiy, E. V. Altynbaev, M. D. Kuchugura, E. G. Yashina, A. S. Sukhanov, V. A. Dyadkin, A. V. Tsvyashchenko, V. A. Sidorov, L. N. Fomicheva, E. Bykova *et al.*, J. Phys.: Condens. Matter **28**, 375401 (2016).